

# Structural and electronic properties of $\text{Mg}_x\text{Zn}_{1-x}\text{O}$ and $\text{Be}_x\text{Mg}_y\text{Zn}_{1-x-y}\text{O}$ alloys from first-principles calculation

QINGHU ZHAO<sup>a</sup>, DEPING XIONG<sup>a,\*</sup>, SHOULI ZHOU<sup>b,\*</sup>, MIAO HE<sup>a</sup>, QU WANG<sup>a</sup>, ZUYONG FENG<sup>a</sup>, WEI ZHANG<sup>a</sup>

<sup>a</sup>*School of Physics and Optoelectronic Engineering, Guangdong University of Technology, Guangzhou 510006, China*

<sup>b</sup>*College of Information Engineering, Zhejiang University of Technology, Hangzhou 310023, China*

Structural and electronic properties of  $\text{Mg}_x\text{Zn}_{1-x}\text{O}$  and  $\text{Be}_x\text{Mg}_y\text{Zn}_{1-x-y}\text{O}$  alloys were studied using the DFT+*U* method. For ternary  $\text{Mg}_x\text{Zn}_{1-x}\text{O}$  alloys, the total energies, lattice constants, and band gaps dependent on Mg content were calculated for wurtzite (*wz*) and rocksalt (*rs*-) structures. By comparing with the total energies of *wz*- and *rs*- $\text{Mg}_x\text{Zn}_{1-x}\text{O}$  alloys, a Mg content of 0.5 was obtained for the phase transition. For quaternary  $\text{BeMgZnO}$ ,  $\text{Be}_x\text{Mg}_{0.5}\text{Zn}_{0.5-x}\text{O}$  alloys possess a wurtzite structure when the Be content is larger than 0.02; the band gap can reach 6.89 eV with a Be content of 0.5.  $\text{Be}_x\text{Mg}_{0.25}\text{Zn}_{0.75-x}\text{O}$  alloys possess a wurtzite structure throughout the Be content range, and their band gaps can reach approximately 7.8 eV when the Be content is 0.75. In addition, the phase diagram for  $\text{Be}_x\text{Mg}_y\text{Zn}_{1-x-y}\text{O}$  alloys was presented for the wurtzite and rocksalt structures.

(Received July 22, 2019; accepted October 21, 2020)

**Keywords:**  $\text{MgZnO}$ , DFT+*U*, First-principles calculation, Electronic properties

## 1. Introduction

The physical properties of group-II oxides are similar to those of group-III nitrides; among them, ZnO is similar to GaN in many aspects. ZnO, which crystallises in a wurtzite structure with a direct band gap of 3.37 eV at room temperature [1], is a new candidate for applications in short-wavelength optoelectronic devices after GaN [2,3]. Further, because of the large exciton binding energy of 60 meV in ZnO, it is expected that ZnO-based light emitters will be even brighter than the corresponding GaN-based light emitters at room temperature. To fabricate highly efficient optoelectronic devices, it is necessary to develop ternary or quaternary alloys, the band gaps of which are larger or smaller than those of the corresponding binary compounds, so as to be capable of preparing heterostructures or quantum wells used in these devices. In the case of ZnO, ternary or quaternary alloys can be formed typically by adding group-II elements, such as Mg, Cd, or Be [4-7]. However, compared to crystallising in a wurtzite structure similar to all group-III nitrides, group-II oxides have different structures at room temperature; for example, BeO and ZnO have a wurtzite structure while MgO has a rocksalt structure. Therefore, when group-II oxides form ternary or quaternary alloys, they suffer from phase instability [8-10], which limits their widespread applications. Therefore, group-II oxides were not greatly used in the semiconductor industry despite increasing research and many publications.

Currently, many researchers have focused on combining MgO or BeO into ZnO to improve the band

gaps of the resulting ternary  $\text{MgZnO}$  and  $\text{BeZnO}$  alloys. It is expected that the direct band gaps can be tuned from 3.37 eV to 7.8 eV for  $\text{MgZnO}$  alloys, and from 3.37 eV to 10.6 eV for  $\text{BeZnO}$  alloys, because the band gaps of ZnO, MgO, and BeO are 3.37 eV, 7.8 eV, and 10.6 eV, respectively. However, the phase segregation of  $\text{Mg}_x\text{Zn}_{1-x}\text{O}$  alloys may occur when  $x > 0.33$  with a maximum direct band gap of approximately 4.0 eV [11]. In contrast,  $\text{BeZnO}$  alloys, because of their high degree of toxicity, remained unexplored until 2006 [12, 13], when studies determined that the achievable band gaps were restricted by the limited solubility of BeO in the ZnO lattice, owing to the large difference in covalent radii between  $\text{Zn}^{2+}$  and  $\text{Be}^{2+}$  [16].

Quaternary  $\text{BeMgZnO}$  alloys can be used to tune the band gaps within a large range without phase segregation and to obtain lattice-matching with ZnO. Their band-gaps in experiments to date have reached approximately 5.0 eV [17, 18]; furthermore, they have exhibited better structural quality than  $\text{BeZnO}$  and  $\text{MgZnO}$  alloys. Currently, theoretical studies of the structural and electronic properties of  $\text{BeMgZnO}$  alloys are rare [3]. Therefore, in this study, we presented the systematic theoretical predictions of the properties of  $\text{Mg}_x\text{Zn}_{1-x}\text{O}$  and  $\text{Be}_x\text{Mg}_y\text{Zn}_{1-x-y}\text{O}$  alloys with Mg or Be content ranging from 0 to 0.1.

## 2. Computational method

The present calculations were carried out using the CASTEP code based on the density function theory (DFT)

[19]. The electron-ion interactions were modelled by ultrasoft pseudopotentials, and the generalized gradient approximation (GGA) was used to describe the exchange-correlation energy between electrons [20]. The valence atomic configurations were  $3d^{10}4s^2$  for Zn,  $2s^22p^4$  for O,  $2s^2$  for Be, and  $3s^2$  for Mg [21]. The wave functions of valence electrons were expanded by a plane-wave basis set, and the cut-off energy was chosen to be 340 eV [22]. For k-point sampling, we used a  $4 \times 4 \times 2$  Monkhorst–Pack grid in the first Brillouin zone, and the convergence threshold was set at  $10^{-6}$  eV for self-consistent iterations. In the optimisation process, all atomic positions for each supercell were fully relaxed until the maximum force on each atom was less than  $0.03 \text{ eV/\AA}$ , the internal stress was below 0.05 GPa, and the displacement tolerance was below  $0.001 \text{ \AA}$ . The calculated band gaps of ZnO, BeO, and MgO were far smaller than their corresponding experimental values, owing to the limitations of the standard DFT [23].

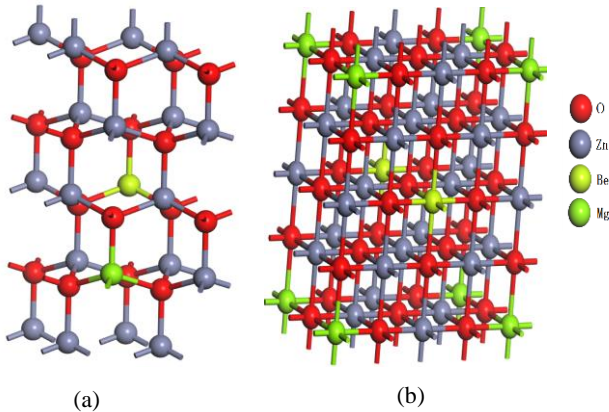


Fig. 1.  $\text{Be}_1\text{Mg}_1\text{Zn}_{14}\text{O}_{16}$  supercell of 32 atoms (a) wurtzite structure, (b) rocksalt structure. Red, grey, yellow, and green spheres represent O, Zn, Be, and Mg atoms, respectively

The DFT+ $U$  method can compensate for the underestimation of the band gap using an orbital dependent term added to the DFT potential [24]. To obtain a more accurate result, in this study, we adopted DFT+ $U$  to

investigate the structural and electronic properties of  $\text{Mg}_x\text{Zn}_{1-x}\text{O}$  and  $\text{Be}_x\text{Mg}_y\text{Zn}_{1-x-y}\text{O}$  alloys; the  $wt$ - and  $rs$ - $\text{Mg}_n\text{Zn}_{16-n}\text{O}_{16}$  and  $\text{Be}_m\text{Mg}_n\text{Zn}_{16-n-m}\text{O}_{16}$  supercells containing 32 atoms were used, as shown in Fig. 1, where  $m, n=0, 1, 2, 3, 4, \dots$ , represent 0, 0.0625, 0.125, 0.1875, ..., of Be and Mg content in the  $\text{Mg}_x\text{Zn}_{1-x}\text{O}$  and  $\text{Be}_x\text{Mg}_y\text{Zn}_{1-x-y}\text{O}$  alloys, respectively. All models were set at  $U_{\text{Zn,d}}=10.5 \text{ eV}$  for Zn 3d orbits and  $U_{\text{o,p}}=0.5 \text{ eV}$  for O 2p orbits. In addition, the scissor operations ( $\Delta=2.0 \text{ eV}$ ) were set according to the difference between the experimental and theoretical band gap. In this manner, we can obtain extremely small differences between the calculated band gaps and experimental data for ZnO, MgO, and BeO.

### 3. Results and discussion

#### 3.1. MgZnO alloys

In normal conditions, ZnO has a wurtzite structure whereas MgO has a rocksalt structure. Therefore,  $\text{Mg}_x\text{Zn}_{1-x}\text{O}$  alloys may have two crystal structures; when  $x$  is small, they are  $wt$ -MgZnO alloys, otherwise they are  $rs$ -MgZnO alloys. In this study, Mg content  $x$  for the structure transition was calculated by comparing the total energies of the two structures [3, 25]. In Table 1, we listed the calculated lattice constants and band gaps for  $wt$ - and  $rs$ -ZnO and MgO, and  $wt$ -BeO. It can be seen that the calculated results are in good agreement with the experimental values, indicating that the DFT+ $U$  method presented herein can reflect the intrinsic properties of ZnO, MgO, and BeO. The same Mg content exhibits different configurations for  $\text{Mg}_n\text{Zn}_{16-n}\text{O}_{16}$  supercells; hence, in table 2, we listed the calculated lattice constants, band gaps, and total energies of  $wt$ - $\text{Mg}_n\text{Zn}_{14}\text{O}_{16}$  supercells for all their possible configurations. The data indicate that the calculated values vary in a small range, and the average values are close to those calculated by the configuration with a large weight value. Therefore, we adopted a special configuration with a large weight for each  $\text{Mg}_n\text{Zn}_{16-n}\text{O}_{16}$  supercell, i.e. the configuration with the Mg atoms distributed homogeneously within the supercells.

Table 1. Calculated lattice constants and band gaps of  $wt$ - and  $rs$ -ZnO, MgO, and  $wt$ -BeO

	ZnO		MgO		BeO	
	wurtzite	rocksalt	wurtzite	rocksalt	Wurtzite	
$a$ (Å)	<i>This work</i>	3.312	4.359	3.241	4.124	2.754
	<i>Other work</i>	3.219 <sup>a</sup>	4.436 <sup>a</sup>	3.259 <sup>a</sup>	4.170 <sup>a</sup>	2.676 <sup>a</sup>
	<i>Exp.</i>	3.258 <sup>b</sup>	-	3.283 <sup>d</sup>	4.22 <sup>e</sup>	2.698 <sup>c</sup>
$c$ (Å)	<i>This work</i>	5.323	-	5.005	-	4.472
	<i>Other work</i>	5.166 <sup>a</sup>	-	4.990 <sup>a</sup>	-	4.348 <sup>a</sup>
	<i>Exp.</i>	5.219 <sup>b</sup>	-	5.095 <sup>d</sup>	-	4.373 <sup>c</sup>
$E_g$ (eV)	<i>This work</i>	3.284	3.199	6.186	7.835	9.20
	<i>Other work</i>	0.74 <sup>c</sup>	-	3.47 <sup>c</sup>	-	7.48 <sup>c</sup>
	<i>Exp.</i>	3.30 <sup>b</sup>	-	6.2 <sup>a</sup>	7.8 <sup>c</sup>	10.6 <sup>e</sup>

a. Ref.[26], b. Ref.[27], c. Ref.[23], d. Ref.[28], e. Ref.[29]

Table 2. Calculated lattice constants, band gaps, and total energies of  $wt\text{-Mg}_x\text{Zn}_{1-x}\text{O}_{16}$  supercell for all their possible configurations

Mg atom coordinates	Symmetry	Weight	Lattice constant		$E_g$ (eV)	Total energy (eV)
			$a$ (Å)	$c$ (Å)		
(1/3,2/3,1/4),(1/3,1/6,1/2)	pm	3	3.302	5.289	3.542	-32917.078
(1/3,2/3,1/4),(2/3,1/3,1/2)	cm	9	3.303	5.295	3.565	-32917.075
(1/3,2/3,1/4),(1/3,1/6,3/4)	p3m1	3	3.302	5.292	3.589	-32917.074
Average			3.303	5.295	3.565	-32917.075

Table 3. Calculated total energies as a function of Mg content for  $wt\text{-Mg}_x\text{Zn}_{1-x}\text{O}$  and  $rs\text{-Mg}_x\text{Zn}_{1-x}\text{O}$  alloys

$x$	0	0.125	0.25	0.375	0.5	0.625	0.75	0.875	1
$wt\text{-}$	-34383.9	-32917.1	-31450.3	-29983.5	-28516.6	-27049.7	-25582.8	-24115.7	-22648.6
$rs\text{-}$	-34380.0	-32914.1	-31448.4	-29982.6	-28516.8	-27050.6	-25584.3	-24118.0	-22651.5

In Table 3, we listed the calculated total energies of  $wt\text{-Mg}_x\text{Zn}_{1-x}\text{O}$  and  $rs\text{-Mg}_x\text{Zn}_{1-x}\text{O}$  dependent on Mg content. The total energies of  $wt\text{-Mg}_x\text{Zn}_{1-x}\text{O}$  alloys are successively lower than, equal to, and larger than that of  $rs\text{-Mg}_x\text{Zn}_{1-x}\text{O}$  with increasing Mg content. Fig. 2 plots the total energy differences between  $wt\text{-}$  and  $rs\text{-Mg}_x\text{Zn}_{1-x}\text{O}$  dependent on the Mg content. The total energy difference is greater than zero when the Mg content is greater than 0.5, i.e. the total energy of  $wt\text{-Mg}_x\text{Zn}_{1-x}\text{O}$  is greater than that of  $rs\text{-Mg}_x\text{Zn}_{1-x}\text{O}$ . According to the principle of minimum energy,  $rs\text{-Mg}_x\text{Zn}_{1-x}\text{O}$  is favourable when  $x > 0.5$ . The critical Mg content of 0.5 obtained herein is in good agreement with the experimental data of 0.51 [29] and theoretical values of 0.50 [3] and 0.48 [30].

Fig. 3 illustrates the lattice constants  $c$  and  $a$  of  $wt\text{-Mg}_x\text{Zn}_{1-x}\text{O}$  vs. Mg content, in which the lattice constant  $a$  is determined by averaging two  $a$  values of the unit cell; there are two slightly different  $a$  values, owing to the asymmetry caused by Mg doping. It can be seen in Fig. 3(a) that the calculated lattice constant  $c$  has a small overestimation compared to the experimental data [29, 31]. The trend of lattice constant  $c$  displays some upward deviation from linearity, whereas in Fig. 3(b), the lattice constant  $a$  displays some downward deviation from linearity. This upward and downward deviations from linearity for lattice constants of  $wt\text{-Mg}_x\text{Zn}_{1-x}\text{O}$  alloys are in good agreement with the results calculated by Gorczyca et al. [18] and Kazuhiro Shimada et al. [32]. Fig. 4 illustrates the lattice constant  $a$  of  $rs\text{-Mg}_x\text{Zn}_{1-x}\text{O}$  as a function of Mg content, in which the trend complies well with Vegard's law and has little nonlinear character. In addition, all the lattice parameters of  $wt\text{-}$  and  $rs\text{-Mg}_x\text{Zn}_{1-x}\text{O}$  decrease gradually with the doping of Mg. This is typically attributed to the differences in the size of the ionic radii between  $\text{Zn}^{2+}$  (0.83 Å) and  $\text{Mg}^{2+}$  (0.78 Å).

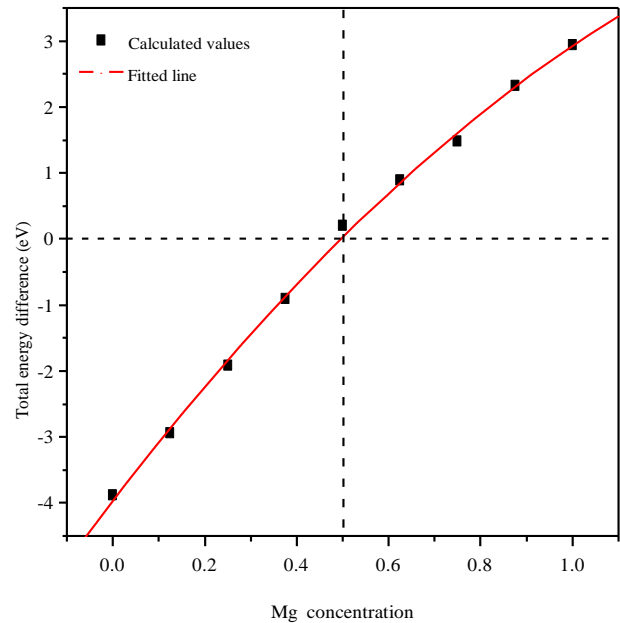
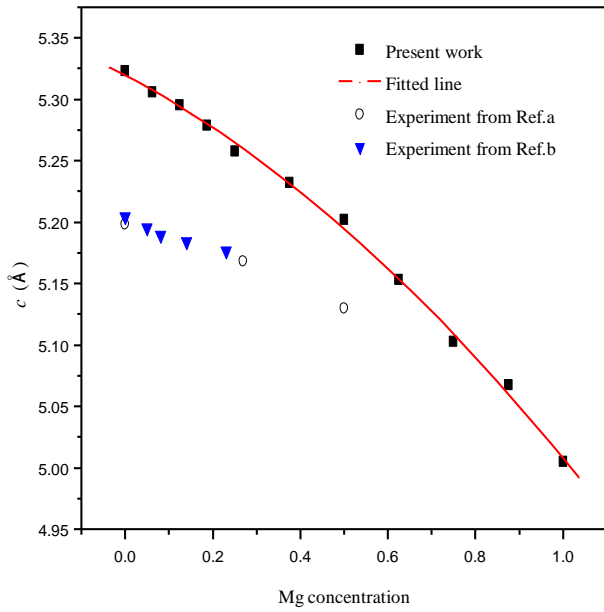
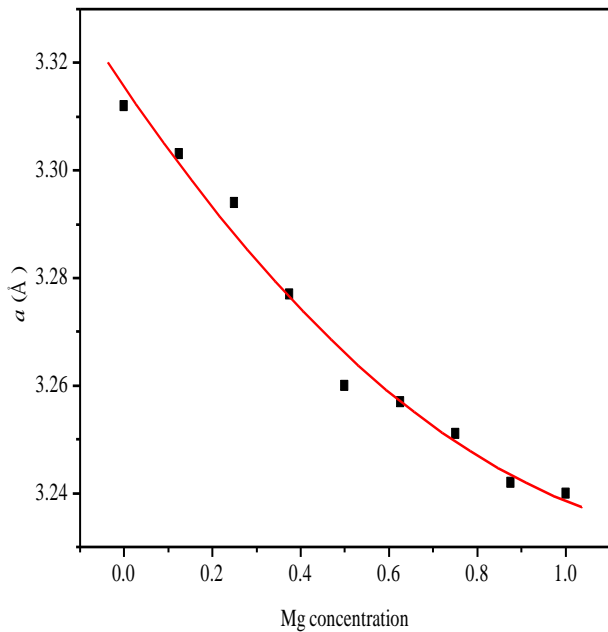


Fig. 2. Total energy differences between  $wt\text{-MgZnO}$  and  $rs\text{-MgZnO}$  alloys as a function of Mg content



(a)



(b)

Fig. 3. Lattice constants (a)  $c$  and (b)  $a$  of  $wt-Mg_xZn_{1-x}O$  alloys as a function of Mg content. Experimental results are from a-Ref.30, b-Ref.32

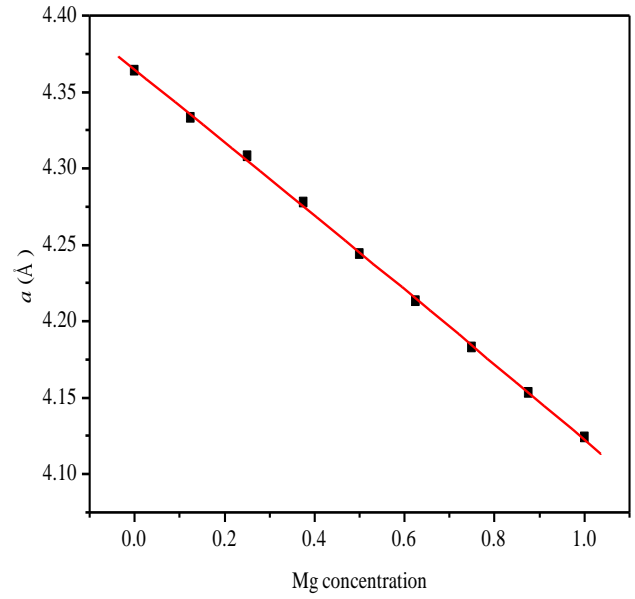


Fig. 4. Lattice constant  $a$  of  $rs-Mg_xZn_{1-x}O$  alloys as a function of Mg content

In Fig. 5, the calculated band gaps of the  $wt$ - and  $rs$ - $Mg_xZn_{1-x}O$  alloys are presented as a function of Mg content, together with the experimental and theoretical data. For stable  $wt$ - $Mg_xZn_{1-x}O$  alloys, Mg content ranges from 0 to 0.5, while for stable  $rs$ - $MgZnO$  alloys it is 0.5–1 [3, 29]. Currently, the available experimental data in Fig. 5 are only in the corresponding stable Mg content range. The plots demonstrate good agreement between the calculated and experimental data [29] and theoretical data [33]. The band gap bowing parameter  $b$ , the deviation from a linear variation of the band gaps, is obtained from the following equation:

$$E_g(x) = (1-x) \cdot E_g(\text{ZnO}) + x \cdot E_g(\text{MgO}) - b(x) \cdot x \cdot (1-x), \quad (1)$$

where  $E_g(x)$  values are the band gaps of  $Mg_xZn_{1-x}O$  alloys, and  $E_g(\text{MgO})$  and  $E_g(\text{ZnO})$  are the band gaps of MgO and ZnO, respectively. In Fig. 5(a), the band gaps of  $wt$ - $MgZnO$  alloys deviate from the linearity very slightly; we fitted them using Eq. (1) by a quadratic function. A small bowing parameter of 0.75 eV was obtained, which is consistent with 0.51 eV and 0.87 eV from other calculations [25, 34]. Conversely, in Fig. 5(b), the band gaps of  $rs$ - $MgZnO$  alloys clearly deviate from linearity, especially in the large Mg content range of 0.5–1. Similarly, a large bowing parameter of 4.6 eV was obtained for  $rs$ - $MgZnO$  alloys, which is roughly consistent with the theoretical value of 3.1 eV [35].

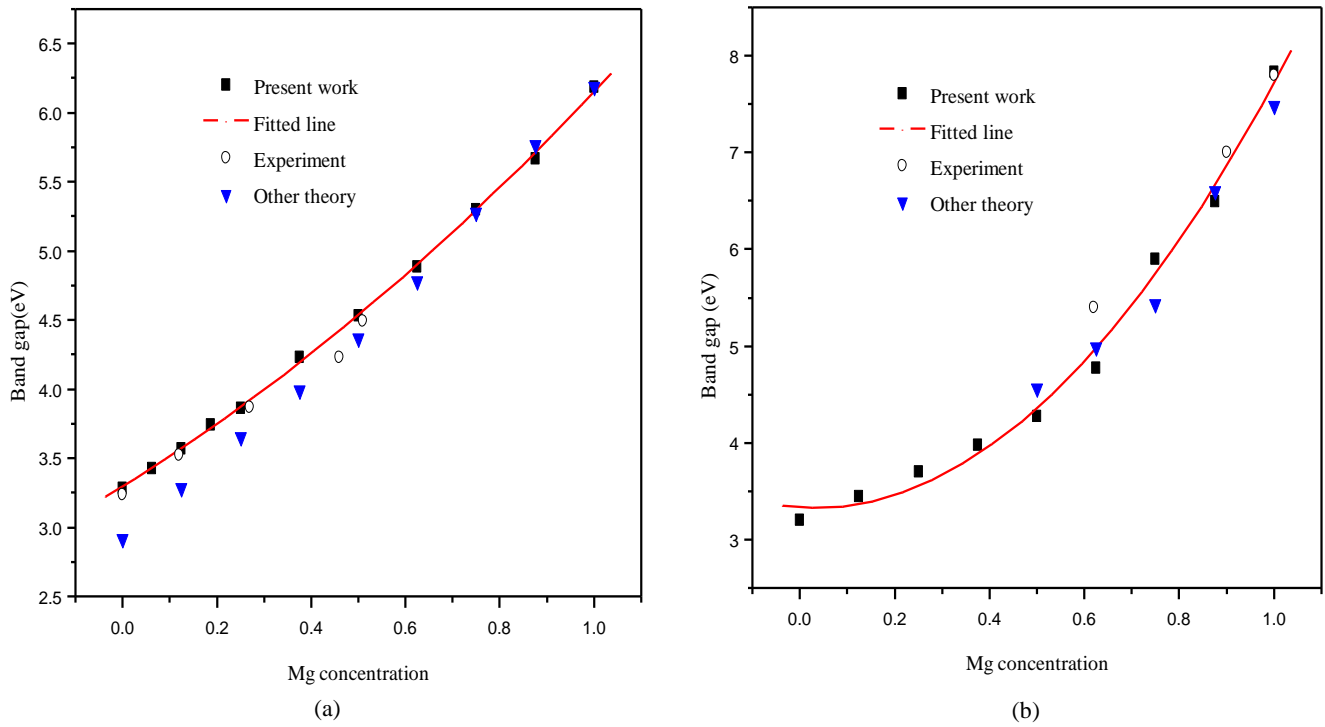


Fig. 5. Band gaps of (a) *wt*-MgZnO and (b) *rs*-MgZnO alloys as a function of Mg content, together with the experiment results from Ref.21 and other theoretical data from Ref.30

### 3.2. Quaternary BeMgZnO alloys

The maximum band gap of the *wt*-Mg<sub>x</sub>Zn<sub>1-x</sub>O alloys is only approximately 4.5 eV because of the limited Mg content, as shown in Fig. 5(a). The quaternary BeMgZnO alloys can be used to obtain a greater band gap with wurtzite structure. BeO itself is in the wurtzite phase with a direct band gap of 10.6 eV. Therefore, we can tune the Be content to achieve a greater band gap for *wt*-BeMgZnO alloys; meanwhile, the lattice constant can be tuned in a greater scale.

Fig. 6(a) illustrates the band gaps of Be<sub>x</sub>Mg<sub>0.5</sub>Zn<sub>0.5-x</sub>O alloys with Be content *x* ranging from 0 to 0.5. The inset shows the total energy differences between the *wt*- and *rs*-Be<sub>x</sub>Mg<sub>0.5</sub>Zn<sub>0.5-x</sub>O alloys dependent on Be content. Be<sub>x</sub>Mg<sub>0.5</sub>Zn<sub>0.5-x</sub>O alloys are in wurtzite phase when the difference is below zero with a Be content ranging from 0.02 to 1. M. Toporkov et al. prepared Be<sub>0.05</sub>Mg<sub>0.5</sub>Zn<sub>0.45</sub>O thin films on (0001) sapphire substrates; the measured optical band gap was 4.77 eV [18], which is in good

agreement with the value of 4.74 eV in Fig. 6(a). In addition, the band gap of Be<sub>x</sub>Mg<sub>0.5</sub>Zn<sub>0.5-x</sub>O alloys can reach 6.89 eV when the Be content is 0.5. As shown further in Fig. 6(a), a large and composition-independent bowing parameter of approximately 4.0 eV was obtained. In Fig. 6(b), the band gaps of Be<sub>x</sub>Mg<sub>0.25</sub>Zn<sub>0.75-x</sub>O alloys are shown as a function of the Be content; the inset is the total energy differences between the *wt*- and *rs*-Be<sub>x</sub>Mg<sub>0.25</sub>Zn<sub>0.75-x</sub>O alloys, and the negative values indicate that the Be<sub>x</sub>Mg<sub>0.25</sub>Zn<sub>0.75-x</sub>O alloys are in the wurtzite phase for any Be content. In Fig. 6(b), the band gap can reach approximately 7.8 eV with a Be content of 0.75, whereas the calculated bowing parameter is 4.7 eV. The large bowing parameters of the Be<sub>x</sub>Mg<sub>y</sub>Zn<sub>1-x-y</sub>O alloys are related to the large differences in covalent radii for Be, Zn, and Mg [3].

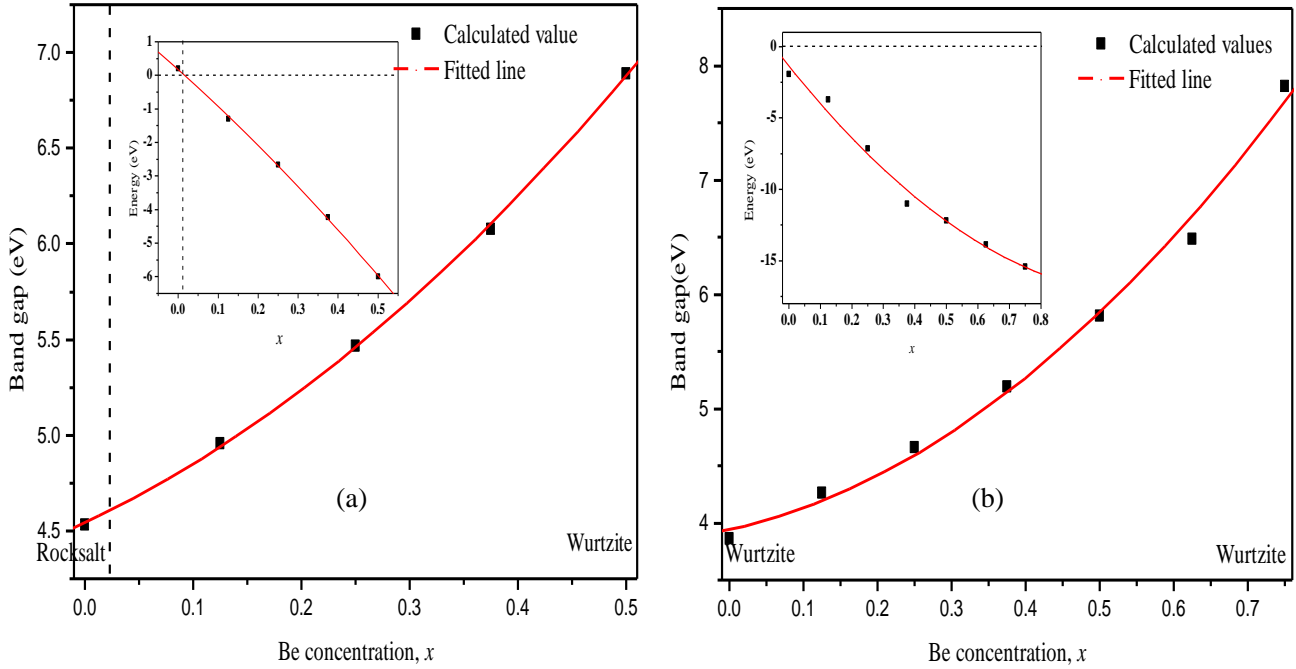


Fig. 6. Band gaps of (a)  $\text{Be}_x\text{Mg}_{0.5}\text{Zn}_{0.5-x}\text{O}$  and (b)  $\text{Be}_x\text{Mg}_{0.25}\text{Zn}_{0.75-x}\text{O}$  alloys as a function of Be content. The inset shows the total energy differences between the corresponding wt- and rs- $\text{BeMgZnO}$  alloys; when the difference is below zero, the alloys are stable in wurtzite structure

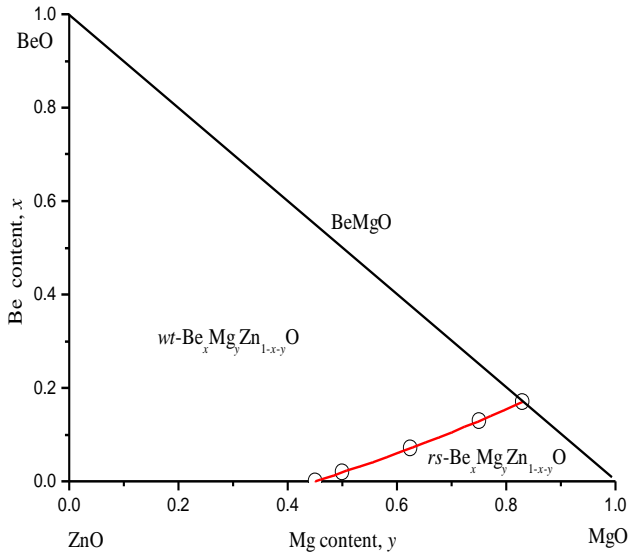


Fig. 7. The phases diagram in which the  $\text{Be}_x\text{Mg}_y\text{Zn}_{1-x-y}\text{O}$  alloys have wurtzite or rocksalt structures. The red line connecting hollow circles is the border-line between two phases

In addition, the total energies of wt- and rs- $\text{Be}_x\text{Mg}_{0.625}\text{Zn}_{0.325-x}\text{O}$ ,  $\text{Be}_x\text{Mg}_{0.75}\text{Zn}_{0.25-x}\text{O}$ , and  $\text{Be}_x\text{Mg}_{1-x}\text{O}$  were calculated. When the total energies of  $\text{BeMgZnO}$  alloys in the two structural phases are equal, the corresponding Be contents were 0.07, 0.13, and 0.17.

Therefore, we can clearly demonstrate the two crystallographic phases for  $\text{Be}_x\text{Mg}_y\text{Zn}_{1-x-y}\text{O}$  alloys in the wurtzite and rock salt phases; as shown in Fig. 7, the red line connecting the hollow circles is the border-line between the two phases.

#### 4. Conclusions

The structural and electronic properties of  $\text{Mg}_x\text{Zn}_{1-x}\text{O}$  and  $\text{Be}_x\text{Mg}_y\text{Zn}_{1-x-y}\text{O}$  alloys were studied by a DFT + $U$  method with the scissor operations ( $\Delta=2.0$  eV). The  $U$  values were set with  $U_{\text{Zn,d}}=10.5$  eV for Zn 3d orbits and  $U_{\text{o,p}}=0.5$  eV for O 2p orbits. In this manner, the band gaps and lattice constants for wt- and rs- $\text{ZnO}$ ,  $\text{MgO}$ , and wt- $\text{BeO}$  were calculated; they are in good agreement with the experimental results, indicating that our calculations are reliable. For ternary  $\text{Mg}_x\text{Zn}_{1-x}\text{O}$  alloys, the total energies, lattice constants, and band gaps depending on Mg content were calculated for the wurtzite and rock salt structures. By comparing with the total energies of wt- and rs- $\text{Mg}_x\text{Zn}_{1-x}\text{O}$  alloys, Mg content was obtained for the phase transition. When Mg content is greater than 0.5, rs- $\text{Mg}_x\text{Zn}_{1-x}\text{O}$  is more favourable than wt- $\text{Mg}_x\text{Zn}_{1-x}\text{O}$ , which is in good agreement with the experimental value of 0.51 and the theoretical value of 0.50. The band gaps of wt- $\text{Mg}_x\text{Zn}_{1-x}\text{O}$  alloys deviate from linearity by a very small amount and have a small bowing parameter of 0.75 eV, whereas the band gaps of rs- $\text{Mg}_x\text{Zn}_{1-x}\text{O}$  alloys have a large bowing parameter of 4.6 eV. The calculated band gaps for the wt- and rs- $\text{Mg}_x\text{Zn}_{1-x}\text{O}$  alloys are in good agreement

with their corresponding experimental values.

Quaternary  $\text{Be}_x\text{Mg}_{0.5}\text{Zn}_{0.5-x}\text{O}$  alloys are in the wurtzite phase when Be content is greater than 0.02. The band gap of  $w\text{-Be}_x\text{Mg}_{0.5}\text{Zn}_{0.5-x}\text{O}$  alloys can reach 6.89 eV with a Be content of 0.5 and a calculated bowing parameter of approximately 4.0 eV.  $\text{Be}_x\text{Mg}_{0.25}\text{Zn}_{0.75-x}\text{O}$  alloys are in the wurtzite phase throughout the range, and the band gap can reach approximately 7.8 eV with a Be content of 0.75 and a calculated bowing parameter of 4.7 eV. In addition, based on the calculated Be and Mg content for the structure transition, the two crystallographic phases were obtained for  $\text{Be}_x\text{Mg}_y\text{Zn}_{1-x-y}\text{O}$  alloys.

### Acknowledgements

This work was supported by the Guangzhou Science and Technology Planning Project of Guangdong Province, China (201604016095), National Natural Science Foundation of China (11874124), and Zhongshan Science and Technology Planning Project of Guangdong Province, China (2017A1008). We also thank the R&D Center for Semiconductor Lighting of Chinese Academy of Sciences for providing us the CASTEP simulation program.

### References

- [1] T. Aoki, Y. Hatanaka, D. C. Look, *Appl. Phys. Lett.* **76**, 3257 (2000).
- [2] Daniel F. Urban, Wolfgang Korner, Christian Elsasser, *Phys Rev. B* **94**, 075140 (2016).
- [3] Gorczyca, H. Teisseyre, T. Suski, N. E. Christensen, A. Svane, *J. Appl. Phys.* **120**, 215704 (2016).
- [4] W. J. Fana, A. P. Abiyasaa, S. T. Tana, S. F. Yua, X. W. Suna, J. B. Xiab, Y. C. Yeoc, M. F. Lic, T. C. Chong, *J. Cryst. Growth* **287**, 28 (2006).
- [5] D. P. Xiong, X. G. Tang, Q. X. Liu, S. L. Zhou, W. R. Zhao, Y. H. Wang, *Vacuum* **89**, 254 (2013).
- [6] Y. R. Ryu, T. S. Lee, H. W. White, *J. Cryst. Growth* **261**, 502 (2004).
- [7] R. de Paiva, J. L. A. Alves, R. A. Nogueira et. al, *Mater. Sci. Eng. B* **93**, 2 (2002).
- [8] I. V. Maznichenko, A. Ernst, M. Bouhassoune, J. Henk, M. Dane, M. Luders, P. Bruno, W. Hergert, I. Mertig, Z. Szotek, W. M. Temmerman, *Phys. Rev. B* **80**, 144101 (2009).
- [9] X. L. Du, Z. X. Mei, Z. L. Liu, Y. Guo, T. C. Zhang et. al., *Adv. Mater.* **21**, 4625 (2009).
- [10] Z. L. Liu, Z. X. Mei, T. C. Zhang, Y. P. Liu, Y. Guo, X. L. Du, A. Hallen, J. J. Zhu, A. Yu Kuznetsov, *J. Cryst. Growth* **311**, 4356 (2009).
- [11] A. K. Sharma, J. Narayan, J. F. Muth, C. W. Teng, C. Jin, A. Kvit, R. M. Kolbas, O. W. Holland, *Appl. Phys. Lett.* **75**, 3327 (1999).
- [12] Y. R. Ryu, T. S. Lee, H. W. White, *J. Cryst. Growth* **261**, 502 (2004).
- [13] Y. R. Ryu, T. S. Lee, J. A. Lubguban, H. W. White et. al., *Appl. Phys. Lett.* **88**, 241108 (2006).
- [14] Mingming Chen, Yuan Zhu, Longxing Su et al., *Appl. Phys. Lett.* **103**, 072104 (2013).
- [15] M. Chen, Y. Zhu, L. Su, Q. Zhang, A. Chen, X. Ji, R. Xiang, X. Gui, T. Wu, B. Pan, Z. Tang, *Appl. Phys. Lett.* **102**, 202103 (2013).
- [16] B. Cordero, V. Gomez, A. E. Platero-Prats, M. Reves, J. Echeverria, E. Cremades, F. Barragan, S. Alvarez, *Dalton Trans.* **21**, 2832 (2008).
- [17] C. Yang, X. M. Li, Y. F. Gu, W. D. Yu, X. D. Gao, Y. W. Zhang, *Appl. Phys. Lett.* **93**, 112114 (2008).
- [18] M. Toporkov, V. Avrutin, S. Okur, N. Izyumskaya, D. Demchenko, J. Volk, D. J. Smith, H. Morkoç, *J. Cryst. Growth* **402**, 60 (2014).
- [19] M. D. Segall, P. J. D. Lindan, M. J. Probert, C. J. Pickard, P. J. Hasnip, S. J. Clark, M. C. Payne, *J. Phys. Condens. Matter.* **14**, 2717 (2002).
- [20] M. C. Payne, M. P. Teter, D. C. Allan, T. A. Arias, J. D. Joannopoulos, *Rev. of Mod. Phys.* **64**, 1045 (1992).
- [21] J. Furthmuller, P. Kachell, F. Bechstedt, G. Kresse, *Phys. Rev. B* **61**, 4576 (2000).
- [22] S. F. Ding, G. H. Fan, S. T. Li, K. Chen, B. Xiao, *Phys. B* **394**, 127 (2007).
- [23] Qiang Xu, Xiu-Wen Zhang, Wei-Jun Fan, Shu-Shen Li, Jian-Bai Xia, *Comput. Matter. Sci.* **44**, 72 (2008).
- [24] R. M. Sheetz, I. Ponomareva, E. Richter, A. N. Andriotis, M. Menon, *Phys. Rev. B* **80**, 195314 (2009).
- [25] D. P. Xiong, X. G. Tang, W. R. Zhao, T. D. Chen, Q. X. Liu, *J. Optoelectron. Adv. M.* **16**(11-12), 1290 (2014).
- [26] Y. Duan, L. Qin, G. Tang, L. Shi, *Eur. Phys. J. B* **66**, 201 (2008).
- [27] U. Ozgur, Ya. I. Alivov, C. Liu, A. Teke, M. A. Reshchikov, Cho, H. Morkoc, *J. Appl. Phys.* **98**, 041301 (2005).
- [28] M. Toporkov, D. O. Demchenko, Z. Zolnai, J. Volk, V. Avrutin, H. Morkoc, U. Ozgur, *J. Appl. Phys.* **119**, 095311 (2016).
- [29] Fikadu Alema, Oleg Ledyae, Ross Miller, Valeria Beletsky, Andrei Osinsky, Winston V. Schoenfeld, *J. Cryst. Growth* **435**, 6 (2016).
- [30] D. Y. Yong, H. Y. He, L. X. Su, Y. Zhu, Z. K. Tang, B. C. Pan, *J. Alloys Comp.* **608**, 197 (2014).
- [31] W. Chunxia, L. Youming, Sh. Dezhen, *Chin. J. Semi.* **25**, 1258 (2004).
- [32] Kazuhiro Shimada, Naomichi Takahashi, Yoshiaki Nakagawa, Tomoyasu Hiramatsu, Hitoshi Kato, *Phys. Rev. B* **88**, 075203 (2013).
- [33] Andre Schleife, Claudia Rodl, Jurgen Furthmuller, Friedhelm Bechstedt, *New Journal of Physics* **13**, 085012 (2011).
- [34] X. F. Fan, H. D. Sun, Z. X. Shen, J.-L. Kuo, Y. M. Lu, *J. Phys. Condens. Matter* **20**, 235221 (2008).
- [35] M. Sanati, G. L. W. Hart, A. Zunger, *Phys. Rev. B.* **68**, 155210 (2003).

\*Corresponding author: depingxiong@gdut.edu.cn,  
zhoushl@zjut.edu.cn